Nanoscale

PAPER

Cite this: *Nanoscale*, 2015, **7**, 8135

Layer number identification of intrinsic and defective multilayered graphenes up to 100 layers by the Raman mode intensity from substrates†

Xiao-Li Li, Xiao-Fen Qiao, Wen-Peng Han, Yan Lu, Qing-Hai Tan, Xue-Lu Liu and Ping-Heng Tan*

Received 8th March 2015,
Accepted 30th March 2015

DOI: 10.1039/c5nr01514f

www.rsc.org/nanoscale

An SiO_2/Si substrate has been widely used to support two-dimensional (2d) flakes grown by chemical vapor deposition or prepared by micromechanical cleavage. The Raman intensity of the vibration modes of 2d flakes is used to identify the layer number of 2d flakes on the SiO_2/Si substrate, however, such an intensity is usually dependent on the flake quality, crystal orientation and laser polarization. Here, we used graphene flakes, a prototype system, to demonstrate how to use the intensity ratio between the Si peak from SiO_2/Si substrates underneath graphene flakes and that from bare SiO_2/Si substrates for the layer-number identification of graphene flakes up to 100 layers. This technique is robust, fast and nondestructive against sample orientation, laser excitation and the presence of defects in the graphene layers. The effect of relevant experimental parameters on the layer-number identification was discussed in detail, such as the thickness of the SiO_2 layer, laser excitation wavelength and numerical aperture of the used objective. This paves the way to use Raman signals from dielectric substrates for layer-number identification of ultrathin flakes of various 2d materials.

Introduction

Single-layered graphene (SLG) has been regarded as a promising material for its high optical transmittance, low resistivity, high chemical stability and mechanical strength.[1,2] Graphene layers can be stacked to form multilayered graphenes (MLGs) in a hexagonal structure, or, less commonly, in a rhombohedral one. Graphene layers in MLGs are coupled with each other by van der Waals interactions. We use the notation NLG to indicate MLG with N layers, and thus 10LG means MLG flakes with 10 layers. In addition, 1LG means SLG. MLGs exhibit many potential applications[3,4] due to their highly tunable electrical properties, such as carrier type or density, rich electronic band structures and various band gaps.[5–7] Therefore, the identification of the layer number (N) of NLG flakes is essential to their fundamental study and practical applications. This is true for multilayered flakes of other two-dimensional crystals. There are several techniques to identify N of NLG flakes. Atomic force microscopy (AFM) is a direct and powerful technique to identify N. However, it is time-consuming and not suitable for a rapid measurement over a large area. Moreover, AFM measurements might be affected by the instrumental offset, substrate roughness and cleanliness of the sample surface. Optical contrast is considered as the most powerful characterization tool for NLG flakes, which correlates sample thickness with the contrast of reflection spectra[8–10] or color difference.[11–13] To precisely identify N, the experimental optical contrast must be compared with the theoretical contrast for different N.[10] The optical contrast technique usually can be applied up to $N = 10$ for a given thickness of the SiO_2 layer (h_{SiO_2}).[8,10]

Raman spectroscopy is one of the most used characterization techniques in carbon science and technology. The Raman spectrum of MLGs consists of the C, D, G and 2D modes. In a MLG comprising N layers, there are $N - 1$ shear (C) modes,[14] where the experimentally-observed C peak with the highest frequency is usually denoted as C_{N1}.[7,15] The D mode which arises from TO phonons around the Brillouin zone edge near K, is active by double resonance.[16] The G peak corresponds to the high-frequency E_{2g} phonon at Γ. The 2D peak is the D peak overtone. The D, G and 2D modes are always present in 1LG.[17] The peak parameters of the C, G and 2D modes can be used to identify N of NLG flakes.[14,17–21] By probing the spectral profile of the 2D mode and peak positions of the C_{N1} modes, one can determine N of Bernal-stacked NLG flakes up to $N = 5$.[14,20] The peak intensity of the G mode, I(G),

State Key Laboratory of Superlattices and Microstructures, Institute of Semiconductors, Chinese Academy of Sciences, Beijing 100083, China. E-mail: phtan@semi.ac.cn

†Electronic supplementary information (ESI) available. See DOI: 10.1039/c5nr01514f

of NLG on the SiO_2/Si substrate is dependent on N because of the multiple reflection interference within the NLG/SiO_2/Si multilayer.[18,19,21] I(G) first increases with the increasing N and then decreases once N is larger than about 20.[18] The non-monotonicity of I(G) dependent on N makes it difficult to determine N only by I(G). In fact, the Raman peaks of NLG are very sensitive to its doping level, defects and stacking orders.[16] With increasing defects and disorder in NLG, the G and 2D peaks are weakened in intensity and broadened in the spectral profile. For example, the 2D mode of rhombohedral-stacked 3LG is quite different from that of Bernal-stacked 3LG in lineshape.[22] All these factors limit the identification of N by the Raman spectrum of NLG flakes themselves.[23] Therefore, how to find a universal method to identify N of NLG flakes with defects and different stacking orders up to tens of layer number is still an open and essential issue.

Here, we proposed a rapid and efficient technique to identify N of intrinsic and defective NLG flakes, which is applicable for both Bernal-stacked and rhombohedral-stacked NLGs. This technique relies on the variation of the Raman mode intensity of the Si peak ($I(Si_G)$) from the SiO_2/Si substrate with N of overlying NLG flakes. $I(Si_G)$ decreases monotonically with increasing N of overlying NLG flakes. This trend is dependent on the SiO_2 film thickness, laser excitation wavelength and numerical aperture (NA) of the objective used. The optimized NA is suggested to be less than 0.5. This technique is applicable for NLG over a wide N range up to ($N \sim 100$), which can also be extended for N determination of other two-dimensional materials deposited onto the SiO_2/Si substrate.

Experimental details

Highly oriented pyrolytic graphite was mechanically exfoliated on the same Si(110) substrate covered with an 89 nm SiO_2 to obtain NLG flakes.[24] The thickness of NLG flakes was pre-estimated by the AFM measurement with a tapping mode. The NLG flakes with $N < 5$ were determined by Raman spectroscopy *via* the lineshape of the 2D peak,[20] and those with $5 \leq N \leq 10$ were confirmed by optical contrast.[8,10] The instrumental offset (σ) of AFM measurements for 1LG is 1.4 nm based on the average of 5 data points.

Raman spectra were measured in back-scattering at room temperature using a Jobin-Yvon HR800 micro-Raman system, equipped with a liquid-nitrogen-cooled CCD, a ×100 objective lens (NA = 0.90) and a ×50 objective lens (NA = 0.45). The excitation wavelengths are 633 nm from a He–Ne laser and 532 nm from a diode-pumped solid-state laser. By monitoring the G peak position,[25] we used a laser power of 0.5 mW to avoid sample heating. The resolution of the Raman system is 0.54 cm^{-1} (at 532 nm) or 0.35 cm^{-1} (at 633 nm) per CCD pixel. For the Raman measurement of each flake, we focused the laser on the bare substrate close to the graphene flake edge to get a maximum intensity of the Si peak by adjusting the focus of the microscope, measured the Si peak from the bare substrate, then moved the laser spot to the graphene flake and measured the Si peak of the substrate covered by graphene flakes and the G peak of the graphene flakes directly. The integration times of 80 s and 200 s were adopted for the Si and G peaks, respectively, to ensure a good signal-to-noise ratio for both the two peaks.

Raman spectra of intrinsic and defective NLG

Fig. 1(a) shows the optical image of a flake containing 1LG, 3LG and 4LG on the SiO_2/Si substrate. Fig. 1(b) is the AFM image of the black rectangle highlighted in Fig. 1(a). The thickness measurements are carried out by two line scans and the corresponding values are also indicated in Fig. 1(b). Although the instrumental offset between 1LG and substrates in different measurements may be different, the thickness difference between two flakes stacked together are quite consistent. Raman spectra at the 1LG and 4LG regions are depicted in Fig. 1(c) in the spectral range of the Si, G and 2D peaks. 1LG and 4LG can be distinguished by the 2D lineshape. The Si signal is from the SiO_2/Si substrate beneath the 1LG and 4LG flakes, whose peak intensity is denoted as $I(Si_G)$. The Si peak intensity from the bare SiO_2/Si substrate is denoted as $I(Si_0)$. It is clear that $I(Si_G)$ at 4LG is weaker than that at 1LG, while the G band intensity (denoted as I_G) of 4LG is stronger than that of 1LG. I(G)/$I(Si_G)$ has been proposed to count N of graphene

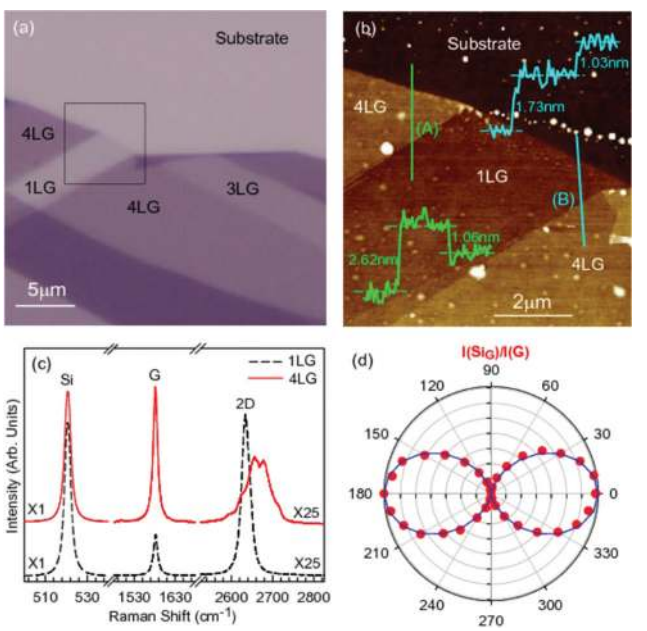

Fig. 1 (a) Optical image of a flake containing 1LG, 3LG and 4LG on an 89 nm SiO_2/Si substrate. (b) AFM image of the sample within the square frame in (a). The height profiles along lines A and B are provided. (c) Raman spectra at 1LG and 4LG regions by 633 nm excitation. (d) The intensity ratio between the Si and G peaks at the 4LG region as a function of the excitation laser polarization angle in the basal plane by 532 nm excitation.

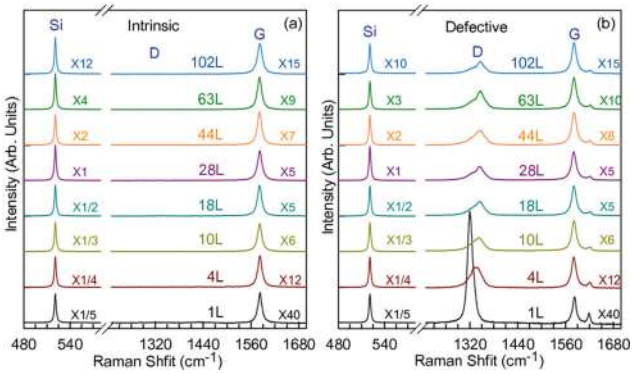

Fig. 2 Raman spectra of intrinsic (a) and defective (b) NLG flakes with specific N in the range of the Si, D and G peaks. N is determined by AFM measurement. The excitation wavelength is 633 nm.

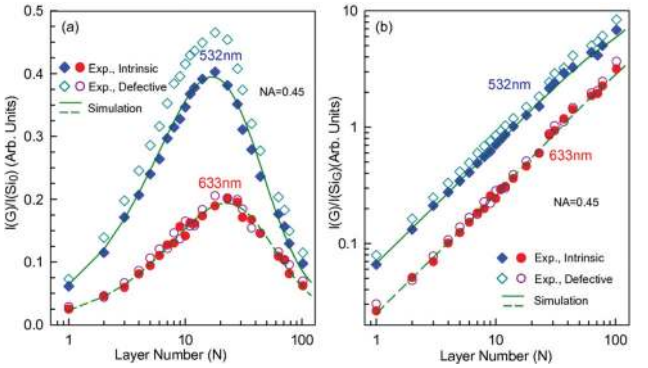

Fig. 3 The experimental and theoretical $I(G)/I(Si_0)$ (a) and $I(G)/I(Si_G)$ (b) as a function of N of NLG flakes. N is determined by AFM measurement. The objective NA is 0.45. The excitation wavelengths of 532 nm and 633 nm are used.

flakes.[21] However, we found that this ratio is dependent on the laser wavelength, grating, laser polarization and the orientation of the SiO_2/Si substrate. As an example, Fig. 1(d) shows the ratio of $I(Si_G)/I(G)$ at 4LG (shown in Fig. 1(a)) on an 89 nm SiO_2/Si(110) substrate as a function of the laser polarization angle (θ) in the basal plane. Although $I(G)$ is constant for different θ, $I(Si_G) \propto \cos^2(\theta)$, sensitive to θ. Thus, it is difficult to identify N of NLG flakes on an SiO_2/Si substrate if the substrate is not Si(111).

$I(Si_0)$ is very strong, usually about 50 times as much as that from bulk graphite. $I(Si_G)$ from the substrate beneath NLG flakes is weaker than $I(Si_0)$ because of the absorption of both excitation power to the substrate and Si Raman signals from the substrate by the top of graphene flakes. Therefore, in principle, Si Raman signals beneath NLG flakes can be considered to identify N of NLG flakes. In order to fully reveal the experimental conditions for this approach, we prepared 22 intrinsic graphene flakes with different N from 1 to 102 from the AFM measurement. Raman spectra of some graphene flakes are depicted in Fig. 2(a) by both objectives with an NA of 0.90 and 0.45. The absence of the D mode indicates high crystal quality of these NLG flakes. $I(Si_G)$ decreases and $I(G)$ first increases up to $N \approx 18$ and then decreases with increasing N. Considering that the real NLG may be defective, after the above measurement, defects were introduced intentionally for all the NLG flakes by ion implantation. C^+ implantation was performed using an LC-4 type system with the dose and kinetic energy of 2×10^{13} cm^{-2} and 80 keV, respectively. After the ion implantation, the D peak at ~1350 cm^{-1} appears in the Raman spectra of the NLG flakes, as depicted in Fig. 2(b), meaning that the NLG flakes become defective. The trend of $I(Si_G)$ and $I(G)$ as a function of N for intrinsic and defective NLG flakes is similar to each other, as shown in Fig. 2.

The Si and G peaks at intrinsic and defective NLG flakes were analyzed by the Lorentz fitting. The peak area intensity of the G peak $I(G)$ normalized by $I(Si_0)$ is summarized in Fig. 3(a) and the peak area intensity ratio $I(G)/I(Si_G)$ is summarized in Fig. 3(b). It clearly shows that $I(G)/I(Si_0)$ reaches a maximum at 18LG for laser excitations of both 532 nm and 633 nm. As shown in Fig. 3, the experimental $I(G)/I(Si_0)$ and $I(G)/I(Si_G)$ of defective NLG flakes significantly diverge from that of intrinsic NLG flakes. Fig. 3(b) shows that $I(G)/I(Si_G)$ increases monotonically with increasing N. $\mathrm{Log}(I(G)/I(Si_G))$ is almost linearly dependent on $\log(N)$. However, in the Raman measurement, we kept the crystal orientation of the Si substrate unchanged for all NLG flakes. Once the crystal orientation of the substrate is changed or the NLG flake is defected or with disorder, it is impossible to identify N for NLG flakes even for $N \leq 15$. A new approach based on Raman spectra is necessary for N determination of NLG flakes.

Optical interference model for the Raman intensity from multilayered structures

Before exploring a new approach for N determination of NLG flakes, we will try to fully understand the behavior of $I(G)$ and $I(G)/I(Si_G)$ as a function of N. Because the Raman intensity in the multilayered structure is determined by multiple reflections at the interfaces and optical interference within the medium, we adopted the multiple reflection interference method, which has been widely used to quantify optical contrast[8,10,26] and Raman intensities[18,19,21,27] of ultrathin flakes of two-dimensional layered materials. When NLG flakes are deposited on SiO_2/Si substrates, the four layered structure can be established, containing air($\tilde{n}_0$), NLG($\tilde{n}_1$, d_1), SiO_2($\tilde{n}_2$, d_2), Si($\tilde{n}_3$, d_3), where $\tilde{n}_i$ and d_i (i = 0, 1, 2, 3) are the complex refractive index and the thickness of each medium, as demonstrated in Fig. 4.

Similar to previous studies,[18,19,21,27] to calculate the intensity of Raman signals from the multilayered structures, one must treat the laser excitation and Raman scattering processes separately. As demonstrated in the square frame in Fig. 4, the laser intensity profile does not decrease monotonically toward

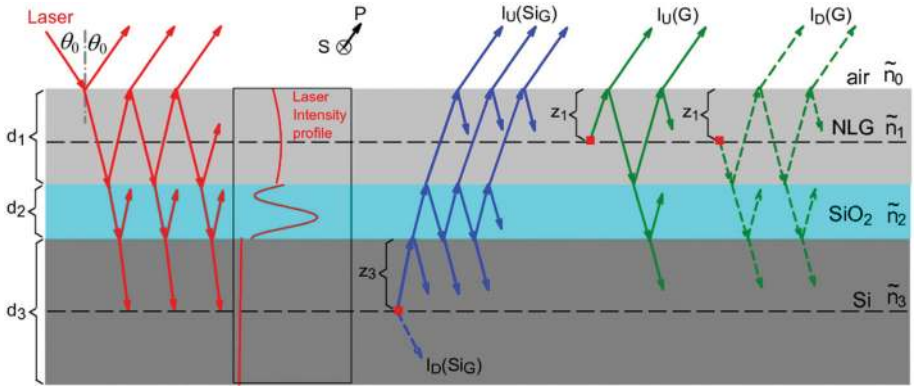

Fig. 4 Schematic diagrams of multiple reflection and optical interference in the multilayered structures containing air, NLG, SiO_2, and Si for the incident laser and out-going Raman signals (the G peak from NLG and the Si peak from the Si substrate). $\tilde{n}_0$, $\tilde{n}_1(d_1)$, $\tilde{n}_2(d_2)$, and $\tilde{n}_3(d_3)$ are the complex refractive indices (thickness) of air, NLG, SiO_2 and Si layers, respectively. The laser intensity distribution along the depth within each medium layer is schematized in the square frame. Two pathways for the emission of Raman signal from silicon substrate and NLG are considered: toward (up,U) and away from (down,D) the NLG surface close to air.

the Si layer. So, the Raman signals from the depth z_1 in the NLG flake and from the depth z_3 in the Si layer will be excited by the laser excitation power at the corresponding depth. The multiple reflection and optical interference are also taken into account in the transition process of Raman signals from the active layers to air. We defined F_L and F_R as the respective enhancement factors for laser excitation and Raman signals, similar to the notation of Yoon *et al.*[19,27] The Raman intensity of a given phonon mode from the medium i can be expressed by integrating over its thickness, d_i, by the following equation:

$$I \propto \int_0^{d_i} |F_L(z_i)F_R(z_i)|^2 dz_i. \quad (1)$$

The transfer matrix formalism can be used to calculate F_L and F_R in the multilayered structures, which has been widely used to calculate the Raman signals and optical contrast of NLG flakes on SiO_2/Si substrates.[10,21,26] In order to take the numerical aperture NA of the objective into account, we calculate contributions from each portion of the laser beam by integrating the incident angle θ from 0 to arcsin(NA). The s-polarization (a transverse electric field, $\vec{E}$, perpendicular to the graphene c-axis) and p-polarization (a transverse magnetic field, $\vec{H}$, associated with an electric field by $\vec{H} = \tilde{n}\vec{E}$) field components[26] are also treated for the transfer matrices. The beam expander is adopted in the optical path to make sure that the laser beam can be regarded as an ideal parallel beam so that the Gaussian intensity distribution of the incident laser beam is ignored in the calculation. Given that the different polarization dependence of the Raman modes of NLG and substrates due to their different lattice symmetries, the Raman tensor $\boldsymbol{R}$ of each phonon mode is also considered. Thus, the total Raman intensity of a Raman mode from the dielectric multilayer is given by integrating over the solid angle (θ,φ for the laser beam and θ',φ' for the Raman signal) of microscope objective and the depth (z_i) in the dielectric layer i:

$$I \propto \int_0^{d_i}\int_0^{\theta'_{max}}\int_0^{2\pi}\int_0^{\theta_{max}}\int_0^{2\pi} \sum_{i=s,p_\perp,p_\parallel}\sum_{j=s',p'_\perp,p'_\parallel} \left|F_L{}^i(z_i,\theta,\varphi)(\vec{e}_R{}^j\cdot\boldsymbol{R}\cdot\vec{e}_L{}^i)F_R{}^j(z_i,\theta',\varphi')\right|^2 \sin\theta\cos\theta d\theta d\varphi \sin\theta'\cos\theta' d\theta' d\varphi' dz_i, \quad (2)$$

where $\vec{e}_R$ and $\vec{e}_L$ are the electric field vectors of the Raman signal and laser excitation at the depth z_i, respectively. In fact, $I(Si_0)$ can be calculated directly based on the above model once the thickness of graphene flakes is set to zero. Calculations of $I(G)$ and $I(Si_G)$ are described in detail in the ESI.†

Based on eqn (2), we calculated $I(G)$ and $I(Si_G)$ as a function of N for NLG flakes on the SiO_2/Si(110) substrate. Because d_2 (thickness of the SiO_2 layer) is a crucial factor[19] in the analysis of the enhancement factors for the Raman intensity, d_2 is taken as 89 nm measured by a spectroscopic ellipsometer in the calculation. Complex refractive indices of graphene, SiO_2 and Si are considered as the common used ones in the previous literature,[28,29] which is dependent on the wavelength λ. The thickness of 1LG is taken to be 0.335 nm. $I(Si_0)$ was also calculated. The ratio (η) of Raman scattering efficiency between the carbon and silicon atoms is used as an adjustable parameter to fit the experimental $I(G)/I(Si_0)$ and $I(G)/I(Si_G)$ in Fig. 3. As depicted in Fig. 3, if η is taken as 1.606 for a 633 nm laser and 0.219 for a 532 nm laser in this work, the theoretical $I(G)/I(Si_0)$ and $I(G)/I(Si_G)$ are in good agreement with the experimental ones of the intrinsic NLG flakes. One must adjust η to make the theoretical data to fit the experimental one of the defective NLG flakes. It is not applicable in the real practise process for N identification because (1) the prepared NLGs are not always free of defects and (2) the Si substrate used for supporting each NLG may be at a random orientation in the chip cutting and in the Raman measurement.

Raman signals from substrate for *N* identification

Because the Si peak from SiO_2/Si substrates is much stronger than the G peak from NLG flakes and is hardly modified by the defects or disorder in NLG flakes, the Si peak can be used as a universal peak for *N* identification of NLG flakes. In order to directly compare the experimental and theoretical data, we calculated $I(Si_G)/I(Si_0)$ as a function of *N* for two laser excitations of 532 nm and 633 nm for NA = 0.45, as depicted in Fig. 5(a) by the solid and dashed lines, respectively. Different excitation wavelengths give different trends for *N*-dependent $I(Si_G)/I(Si_0)$, however, for both the excitation wavelengths, $I(Si_G)/I(Si_0)$ decreases monotonically with the increasing *N* of NLG flakes. With *N* increasing from 1 to 10, $I(Si_G)/I(Si_0)$ decreases from ~0.95 to ~0.55, which is enough for *N* determination. According to the two theoretical curves, we can determine *N* of each NLG flake based on the experimental data for each excitation wavelength. We considered the round number of the average *N* determined by 532 nm and 633 nm excitations as the final *N* for each intrinsic or defective NLG flake. Then, we summarized $I(Si_G)/I(Si_0)$ as a function of *N* only determined by Raman measurements in Fig. 5(a), as shown by diamonds, squares and triangles. Based on this new approach of *N* identification, the *N* deviation given by 532 nm and 633 nm excitations is very small, almost zero for $N \leq 15$, less than 1 for $16 \leq N \leq 40$, and less than 3 for $41 \leq N \leq 100$. *N* determined by Raman measurements is compared with the thickness (h) of the NLG flakes by AFM measurements, as shown in the inset to Fig. 5(a). We used $h = h_0 + d_C N$ to fit the data, giving an AFM offset (h_0) of 1.4 nm and a layer spacing distance (d_C) of 0.333 nm. The *N* deviation between Raman measurement and AFM fitting can be as large as 2 for 21LG, 3 for 34LG and 5 for 66LG.

$I(Si_G)/I(Si_0)$ was calculated for three NA values of 0, 0.72 and 0.9 excited by the 633 nm excitation, as shown in Fig. 5(b) by dash-dotted, solid and dashed lines, respectively. $I(Si_G)/I(Si_0)$ is also dependent on NA. The error of *N* determination based on theoretical NA = 0 for experimental NA = 0.9 can be up to 15%. Fig. 5(b) shows $I(Si_G)/I(Si_0)$ measured by an objective with NA = 0.9, which is found to be consistent with the theoretical one of NA = 0.72. The reduction of effective NA in this experiment is similar to the previous reports[10] on the optical contrast of graphene flakes on SiO_2/Si substrates. This reduction can result in an uncertainty of 1 for $N < 10$ and of up to 7 for $N = 100$.

For practical application, $I(Si_G)/I(Si_0)$ was calculated for several typical h_{SiO_2}. Fig. 6(a) depicts $I(Si_G)/I(Si_0)$ for NLG flakes on the substrate with h_{SiO_2} = 290 nm, 300 nm, 90 nm and 100 nm. It is evident that only a variation of 10 nm for h_{SiO_2} can introduce a significant change on the *N*-dependent curve, which results in a large error for *N* determination for a thicker NLG flake. This suggests that precise h_{SiO_2} is very important before *N* determination for NLG flakes on SiO_2/Si substrates by $I(Si_G)/I(Si_0)$, similar to the case of *N* determination *via* optical contrast. The difference between $I(Si_G)/I(Si_0)$ excited by 532 nm and 633 nm excitations for h_{SiO_2} = 300 nm depicted in Fig. 6(a) is more significant than that for h_{SiO_2} = 89 nm as shown in Fig. 5(a). However, for an excitation of 532 nm, the calculated $I(Si_G)/I(Si_0)$ as a function of h_{SiO_2} for h_{SiO_2} = 290 nm, 300 nm, 90 nm and 100 nm are almost identical to each other, as demonstrated in Fig. 6(b). The theoretical error for *N* determination induced by the difference of the four curves can be as small as 1 up to 80LG. Thus, 532 nm excitation is a good option for *N* determination of NLG flakes on SiO_2/Si substrates of 285 nm < h_{SiO_2} < 305 nm or 90 nm < h_{SiO_2} < 110 nm.

The advantages of the *N* identification based on the Si peak intensity from substrates are summarized here: (1) the Raman intensity from Si substrates can be so intense up to tens of thousands per second that the signal-to-noise ratio of the measured $I(Si_G)/I(Si_0)$ can be very high even for thick graphene flakes. (2) In contrast to $I(G)/I(Si_G)$, this technique does not need to introduce an undetermined Raman efficiency of

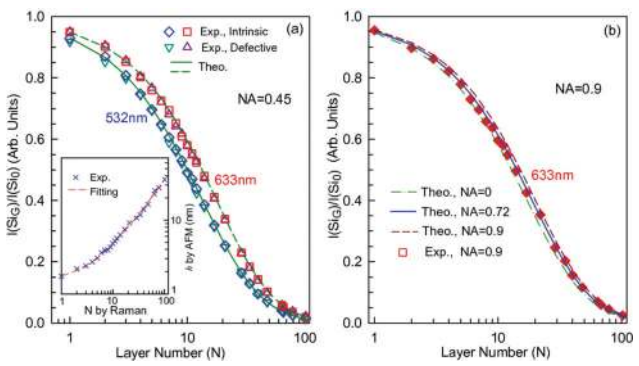

Fig. 5 (a) The theoretical curves and experimental data of $I(Si_G)/I(Si_0)$ for 532 nm and 633 nm excitations and NA = 0.45. The thickness of NLG flakes measured by AFM as a function of *N* identified by Raman measurement is plotted in the inset. (b) $I(Si_G)/I(Si_0)$ as a function of *N* by the 633 nm excitation for different NA: experimental data (squares, NA = 0.9), theoretical curves (lines, NA = 0, 0.72, 0.9).

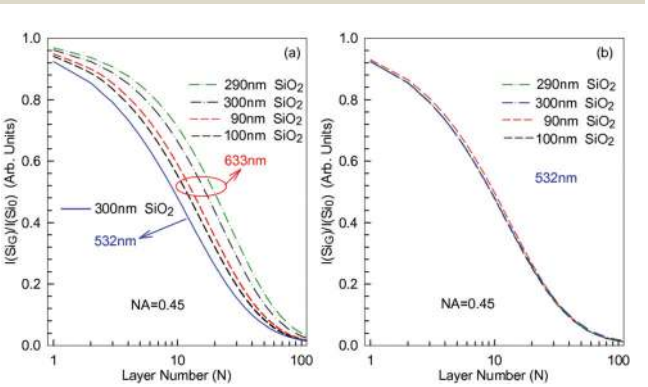

Fig. 6 (a) The calculated $I(Si_G)/I(Si_0)$ excited by a 633 nm excitation as a function of *N* for different h_{SiO_2} and that of h_{SiO_2} = 300 nm excited by a 532 nm excitation for a comparison. (b) The calculated $I(Si_G)/I(Si_0)$ excited by a 532 nm excitation as a function of *N* for different h_{SiO_2}. The NA of the objective is 0.45.

different atoms in the intensity calculation for the corresponding Raman modes. (3) Because $I(Si_G)$ and $I(Si_0)$ are from the same Si substrate, it makes the measured value $I(Si_G)/I(Si_0)$ robust for any substrate orientation and laser polarization. (4) $I(Si_G)/I(Si_0)$ is not affected by slight disorder as shown in Fig. 5(a) and even doping or adsorption if they do not significantly change the complex refractive index of graphene flakes. (5) The N identification based on Raman spectroscopy offers a high spatial resolution for other optical techniques, such as optical contrast.

There are several factors to be noted in the N identification of NLG flakes based on $I(Si_G)/I(Si_0)$: (1) in order to ensure the accuracy of N identification, a microscope objective with NA 0.45 is suggested, and smaller effective NA should be considered for larger NA, as shown in Fig. 5(b). The reason may be that Raman signals in the entire field of view were not fully collected.[26] (2) h_{SiO_2} must be confirmed by initial measurement by a spectroscopic ellipsometer or other techniques[30] because $I(Si_G)/I(Si_0)$ is very sensitive to h_{SiO_2}. (3) If the diameter of a laser beam with a Gaussian intensity profile is comparable or smaller than that of the objective aperture, the stronger intensity at the center of the laser beam will result in a smaller effective NA in the theoretical calculation to fit the experimental results.

Conclusions

We demonstrated a robust, fast and nondestructive method to identify the layer number of graphene flakes on SiO_2/Si substrates for any substrate orientation and laser polarization. The intensity ratio of the Si peak from SiO_2/Si substrates underneath graphene flakes to that from bare SiO_2/Si substrates is used as a probe for the layer number. The high signal-to-noise ratio make this method robust against the presence of defects in the graphene layers. This technique can be extended for layer-number identification of ultrathin flakes of other 2d materials, such as semimetals ($NiTe_2$ and VSe_2), semiconductors (WS_2, WSe_2, MoS_2, $MoSe_2$, $MoTe_2$, TaS_2, $RhTe_2$ and $PdTe_2$), insulators (HfS_2), superconductors (NbS_2, $NbSe_2$, $NbTe_2$, and $TaSe_2$) and topological insulators (Bi_2Se_3 and Bi_2Te_3).[31]

Acknowledgements

We acknowledge support from the National Natural Science Foundation of China, grants 11225421, 11434010 and 11474277.

Notes and references

1 A. K. Geim and K. S. Novoselov, *Nat. Mater.*, 2007, **6**, 183.
2 F. Bonaccorso, Z. Sun, T. Hasan and A. C. Ferrari, *Nat. Photonics*, 2010, **4**, 611.
3 J. B. Oostinga, H. B. Heersche, X. Liu, A. F. Morpurgo and L. M. K. Vandersypen, *Nat. Mater.*, 2008, **7**, 151.
4 M. F. Craciun, S. Russo, M. Yamamoto, J. B. Oostinga, A. F. Morpurgo and S. Tarucha, *Nat. Nanotechnol.*, 2009, **4**, 383.
5 B. Partoens and F. M. Peeters, *Phys. Rev. B: Condens. Matter*, 2006, **74**, 075404.
6 A. Grueneis, C. Attaccalite, L. Wirtz, H. Shiozawa, R. Saito, T. Pichler and A. Rubio, *Phys. Rev. B: Condens. Matter*, 2008, **78**, 205425.
7 J.-B. Wu, X. Zhang, M. Ijäs, W.-P. Han, X.-F. Qiao, X.-L. Li, D.-S. Jiang, A. C. Ferrari and P.-H. Tan, *Nat. Commun.*, 2014, **5**, 5309.
8 Z. H. Ni, H. M. Wang, J. Kasim, H. M. Fan, T. Yu, Y. H. Wu, Y. P. Feng and Z. X. Shen, *Nano Lett.*, 2007, **7**, 2758.
9 P. Blake, E. W. Hill, A. H. C. Neto, K. S. Novoselov, D. Jiang, R. Yang, T. J. Booth and A. K. Geim, *Appl. Phys. Lett.*, 2007, **91**, 063124.
10 W. P. Han, Y. M. Shi, X. L. Li, S. Q. Luo, Y. Lu and P. H. Tan, *Acta Phys. Sin.*, 2013, **62**, 110702.
11 L. Gao, W. Ren, F. Li and H.-M. Cheng, *ACS Nano*, 2008, **2**, 1625.
12 H. Li, J. Wu, X. Huang, G. Lu, J. Yang, X. Lu, Q. Zhang and H. Zhang, *ACS Nano*, 2013, **7**, 10344.
13 Y.-F. Chen, D. Liu, Z.-G. Wang, P.-J. Li, X. Hao, K. Cheng, Y. Fu, L.-X. Huang, X.-Z. Liu and W.-L. Zhang, *J. Phys. Chem. C*, 2011, **115**, 6690.
14 P. H. Tan, W. P. Han, W. J. Zhao, Z. H. Wu, K. Chang, H. Wang, Y. F. Wang, N. Bonini, N. Marzari, N. Pugno, G. Savini, A. Lombardo and A. C. Ferrari, *Nat. Mater.*, 2012, **11**, 294.
15 P.-H. Tan, J.-B. Wu, W.-P. Han, W.-J. Zhao, X. Zhang, H. Wang and Y.-F. Wang, *Phys. Rev. B: Condens. Matter*, 2014, **89**, 235404.
16 A. C. Ferrari and D. M. Basko, *Nat. Nanotechnol.*, 2013, **8**, 235–246.
17 A. C. Ferrari, J. C. Meyer, V. Scardaci, C. Casiraghi, M. Lazzeri, F. Mauri, S. Piscanec, D. Jiang, K. S. Novoselov, S. Roth and A. K. Geim, *Phys. Rev. Lett.*, 2006, **97**, 187401.
18 Y. Y. Wang, Z. H. Ni, Z. X. Shen, H. M. Wang and Y. H. Wu, *Appl. Phys. Lett.*, 2008, **92**, 043121.
19 D. Yoon, H. Moon, Y.-W. Son, J. S. Choi, B. H. Park, Y. H. Cha, Y. D. Kim and H. Cheong, *Phys. Rev. B: Condens. Matter*, 2009, **80**, 125422.
20 W. J. Zhao, P. H. Tan, J. Zhang and J. Liu, *Phys. Rev. B: Condens. Matter*, 2010, **82**, 245423.
21 Y. K. Koh, M.-H. Bae, D. G. Cahill and E. Pop, *ACS Nano*, 2011, **5**, 269.
22 C. H. Lui, Z. Li, Z. Chen, P. V. Klimov, L. E. Brus and T. F. Heinz, *Nano Lett.*, 2011, **11**, 164–169.
23 A. C. Ferrari, *Solid State Commun.*, 2007, **143**, 47.
24 K. S. Novoselov, D. Jiang, T. Booth, V. V. Khotkevich, S. M. Morozov and A. K. Geim, *Proc. Natl. Acad. Sci. U. S. A.*, 2005, **102**, 10451.

25 P. Tan, Y. Deng, Q. Zhao and W. Cheng, *Appl. Phys. Lett.*, 1999, **74**, 1818–1820.
26 C. Casiraghi, A. Hartschuh, E. Lidorikis, H. Qian, H. Harutyunyan, T. Gokus, K. S. Novoselov and A. C. Ferrari, *Nano Lett.*, 2007, **7**, 2711.
27 S.-L. Li, H. Miyazaki, H. Song, H. Kuramochi, S. Nakaharai and K. Tsukagoshi, *ACS Nano*, 2012, **6**, 7381.
28 V. G. Kravets, A. N. Grigorenko, R. R. Nair, P. Blake, S. Anissimova, K. S. Novoselov and A. K. Geim, *Phys. Rev. B: Condens. Matter*, 2010, **81**, 155413.
29 E. D. Palik, *Handbook of Optical Constants of Solids*, Academic Press, New York, 1985.
30 Y. Lu, X.-L. Li, X. Zhang, J.-B. Wu and P.-H. Tan, *Sci. Bull.*, 2015, DOI: 10.1007/s11434-015-0774-3.
31 A. K. Geim and I. V. Grigorieva, *Nature*, 2013, **499**, 419.